MNRAS 000, 1–14 (2021) Preprint 1 April 2021 Compiled using MNRAS LATEX style file v3.0

Two c's in a pod: Cosmology independent measurement of the Type Ia supernova colour - luminosity relation with a sibling pair

Rahul Biswas,[1]★ Ariel Goobar,[1]† Suhail Dhawan,[1,2] Steve Schulze,[1] Joel Johansson,[1] Eric C. Bellm,[3] Richard Dekany,[4] Andrew J. Drake,[5] Dmitry A. Duev,[5] Christoffer Fremling[5] Matthew Graham,[5] Young-Lo Kim,[6] Erik C. Kool,[7] Shrinivas R. Kulkarni,[5] Ashish A. Mahabal,[5,8] Daniel Perley,[9] Mickael Rigault,[6] Ben Rusholme,[10] Jesper Sollerman,[7] David L. Shupe,[10] Matthew Smith,[6] Richard S. Walters[4]

[1]*Oskar Klein Centre, Department of Physics, Stockholm University, SE 106 91 Stockholm, Sweden*
[2]*Kavli Institute for Cosmology, University of Cambridge, Madingley Road, Cambridge CB3 0HA, UK*
[3]*DIRAC Institute, Department of Astronomy, University of Washington, 3910 15th Avenue NE, Seattle, WA 98195, USA*
[4]*Caltech Optical Observatories, California Institute of Technology, Pasadena, CA 91125, USA*
[5]*Division of Physics, Mathematics, and Astronomy, California Institute of Technology, Pasadena, CA 91125, USA*
[6]*Univ Lyon, Univ Claude Bernard Lyon 1, CNRS, IP2I Lyon / IN2P3, IMR 5822, F-69622, Villeurbanne, France*
[7]*Department of Astronomy, Oskar Klein Centre, Stockholm University, Albanova, 10691 Stockholm, Sweden*
[8]*Center for Data Driven Discovery, California Institute of Technology, Pasadena, CA 91125, USA*
[9]*Astrophysics Research Institute, Liverpool John Moores University, IC2, Liverpool Science Park, 146 Brownlow Hill, Liverpool L3 5RF, UK*
[10]*IPAC, California Institute of Technology, 1200 E. California Blvd, Pasadena, CA 91125, USA*

Accepted XXX. Received YYY; in original form ZZZ

ABSTRACT

Using Zwicky Transient Facility (ZTF) observations, we identify a pair of "sibling" Type Ia supernovae (SNe Ia), i.e., hosted by the same galaxy at $z = 0.0541$. They exploded within 200 days from each other at a separation of $0.6''$ corresponding to a projected distance of only 0.6 kpc. Performing SALT2 light curve fits to the *gri* ZTF photometry, we show that for these equally distant 'standardizable candles", there is a difference of 2 magnitudes in their rest frame B-band peaks, and the fainter SN has a significantly red SALT2 colour $c = 0.57 \pm 0.04$, while the stretch values x_1 of the two SNe are similar, suggesting that the fainter SN is attenuated by dust in the interstellar medium of the host galaxy. We use these measurements to infer the SALT2 colour standardization parameter, $\beta = 3.5 \pm 0.3$, independent of the underlying cosmology and Malmquist bias. Assuming the colour excess is entirely due to dust, the result differs by 2σ from the average Milky-Way total-to-selective extinction ratio, but is in good agreement with the colour-brightness corrections empirically derived from the most recent SN Ia Hubble-Lemaitre diagram fits. Thus we suggest that SN "siblings", which will increasingly be discovered in the coming years, can be used to probe the validity of the colour and lightcurve shape corrections using in SN Ia cosmology while avoiding important systematic effects in their inference from global multi-parameter fits to inhomogeneous data-sets, and also help constrain the role of interstellar dust in SN Ia cosmology.

Key words: AT 2019lcj,SN 2020aewj,dust, extinction, observations

1 INTRODUCTION

The discovery of the late-time accelerated expansion of the universe using Supernovae of Type Ia (SNe Ia) as cosmological yardsticks (Riess et al. 1998; Perlmutter et al. 1999) had a profound impact on our understanding of the cosmic composition. The pioneering work of the Supernova Cosmology Project and the High-z Supernova Search Team was followed by many efforts to improve the use of SNe Ia in cosmology with the purpose to better understand the nature of dark energy (see Goobar & Leibundgut 2011, for a review). Essential for the standardization of SNe Ia to obtain precise distances are the corrections for the lightcurve shape-brightness relation (Phillips 1993) and the colour-brightness relation (Tripp 1998). In recent

★ E-mail: rbiswas4@gmail.com
† E-mail: ariel@fysik.su.se

years, most SNe Ia cosmological samples are analyzed in the SALT2 lightcurve framework (Guy et al. 2005, 2007, 2010). The distance modulus μ is corrected for lightcurve shape (x_1) and colour (c) as

$$\mu = m - M + \alpha \cdot x_1 - \beta \cdot c,$$

where α and β are constants, whose values are determined by fitting to a Hubble-Lemaitre diagram. The colour measurement, c, which corresponds approximately to $E(B-V)$ where the SALT2 template SED is used as reference is thus multiplied by an empirically derived parameter β, the topic of this work. In the SALT2 framework, the absolute magnitude M_B in rest-frame B-band is used as the anchoring point.

The SALT2 model performs standardization in a two step process. First the SALT2 model is fitted to the light curve data of each supernova. These parameters and uncertainties are then used to simultaneously determine the parameters α and β along with the cosmology. Traditionally, this was performed for each cosmological model (and possibly) with complementary data if desired. This made the standardized distance moduli (through the values of α and β) dependent on both the choice of the cosmological model used, and the complementary data. The use of SALT2mu (Marriner et al. 2011), which uses piece-wise continuous cosmological distance moduli functions of ΛCDM in different redshift bins, ameliorates the cosmological model dependence. More importantly, it paves the way for a generalized intrinsic scatter model in the form of a covariance between the parameters $\{m, x_1, c\}$. Over the past decade, it has been established that there is a significant environmental dependence of the distance modulus on the the properties of the host galaxy beyond the Tripp Standardization (Kelly et al. 2010; Sullivan et al. 2010; Lampeitl et al. 2010; Childress et al. 2013; Rigault et al. 2015, 2020; Kelsey et al. 2021). Moreover, it has been realized that selection effects in observational surveys result in incompleteness in the distribution of SNe Ia properties due to interaction with the intrinsic dispersion, and affect the inferred values of β. In cosmological analyses (Kessler et al. 2009; Betoule et al. 2014; Brout et al. 2019) these are usually corrected through a set of bias corrections terms (Mosher et al. 2014; Kessler & Scolnic 2017; Kessler et al. 2019; Popovic et al. 2021) based on simulations. Such simulations require detailed inputs of population models inferred from the data (Kessler et al. 2013; Scolnic & Kessler 2016) and a detailed description of the observational procedure. Given the complexity of such a program and the importance of these parameters to cosmology, complementary checks which do not involve many of such effects like environmental dependence or population models are important cross-checks.

Concerns have been raised that the colour-brightness parameter β derived from cosmological analysis may be biased due to selection effects, procedural mistakes, degeneracies with other parameters in the global fits, redshift uncertainties, K-corrections, calibration errors, and possibly even Milky-Way extinction errors. Indeed, over time and for different samples, the reported best fit value of β has varied from 1.57 ± 0.15 (Astier et al. 2006), 2.47 ± 0.06 (Suzuki et al. 2012), to $\beta \approx 3.0$, reported by Scolnic et al. (2018). Recently, Brout & Scolnic (2021) suggested that the extinction properties of SNe Ia depend on the host galaxy stellar mass, thus providing further uncertainty in the reported single "universal" values of β (but see Thorp et al. 2021, for a different conclusion).

Assuming the colour excess is entirely due to extinction by interstellar dust in the host galaxy of the supernovae, β corresponds to the total-to-selective extinction parameter, R_B, following the analogy of Milky-Way extinction (see e.g., Cardelli et al. 1989). However, when β is fitted using the ensemble of low and high-z SNe Ia to minimize the scatter in the Hubble-Lemaitre diagram residuals, its value comes out to be significantly lower than $\beta \sim R_B \approx 4.1$, the Milky-Way average value (Astier et al. 2006; Kessler et al. 2009; Amanullah et al. 2010; Suzuki et al. 2012; Betoule et al. 2014; Scolnic et al. 2018). Focusing on the most recent analyses, Betoule et al. (2014) find $\beta = 3.101 \pm 0.075$ based on a sample of 740 SN Ia and Scolnic et al. (2018) find $\beta = 3.030 \pm 0.063$ when they extend the sample with newer discoveries, totalling 1048 SNe with similar lightcurve selections. Since only objects with moderate colour have been kept in the samples used for cosmology, $c \leq 0.3$, it has been argued in those studies that the low values of β could be mainly due to intrinsic colour variations (see also Chotard et al. 2011). It has also been suggested that dust localized to the circumstellar environment could cause non-standard extinction (Wang 2005; Goobar 2008). The latter suggestion has been explored studying the wavelength dependent attenuation of SN 2014J, a highly reddened SN Ia in the nearby galaxy M82 which also showed non-standard extinction (Goobar et al. 2014; Amanullah et al. 2014; Foley et al. 2014), and through searches of emission from heated circumstellar dust (Maeda et al. 2015; Johansson et al. 2017). The colour relations of samples of nearby reddened SNe Ia have been reporting "non-standard" extinction laws for over a decade (see e.g, Nobili & Goobar 2008), and have recently been expanded with observations ranging from UV to NIR (Burns et al. 2014; Amanullah et al. 2015). The conclusion from these studies is that extinction by circumstellar dust likely plays a minor role in the observed colour-brightness relation of SNe Ia, and that a diverse population of dust in the interstellar medium of other galaxies is required to explain the observations, even after intrinsic colour variations are taken into account. An intriguing possibility that has been put forward is that dust grains may be fragmented by collisions between dust clouds, as these are accelerated by radiation pressure from the SN itself (Hoang 2017; Bulla et al. 2018), or by radiation in the interstellar medium (Hoang 2021).

While the well-measured nearby SNe Ia, too close to be in the Hubble flow, were able to provide supporting evidence for the "non-standard" wavelength dependence of attenuation, they could not probe the absolute attenuation. This work bridges the efforts between the local and cosmological efforts to study the relation between colour excess and brightness attenuation for SNe Ia.

As time domain astronomy surveys get larger and run for longer survey durations, they can find rare objects. Multiple SNe Ia occurring in the same host galaxy, known as siblings, are rare but were not unheard of. Recent surveys have increased the number of such siblings, allowing ensemble level questions to be addressed through them (Scolnic et al. 2020; Burns et al. 2020), which use the Dark Energy Survey and CSP data to discuss to what extent sibling supernovae share common properties. In this work we present a case that circumvents all of the above mentioned shortcomings. As the Zwicky Transient Facility (Bellm et al. 2019a) scans the sky with unprecedented speed and depth (Graham et al. 2019) it has the potential to discover rare events, including sibling supernovae. For a more comprehensive discussion on sibling supernovae found in ZTF, see Graham et al., 2021, (in prep), as well as a potential event reported in Soraisam et al. (2021). In this work, we use a particular set of sibling SNe Ia , found at nearly identical positions within a year, but with significantly different observed

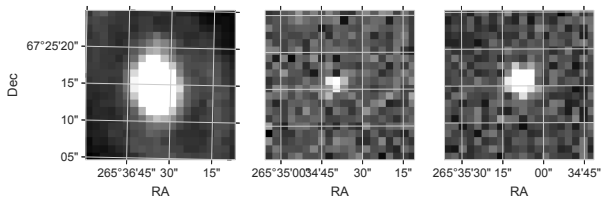

Figure 1. From left to right: g-band postage stamps in of the reference image (i.e. the host galaxy) centred at AT 2019lcj, the difference image for AT 2019lcj for the science image on July 16, 2019, and the difference image for SN 2020aewj centred on its position using the science image on February 7, 2020. In both cases, the SNe were close to lightcurve maximum.

flux and colours to constrain the parameter β in the Tripp relation, related to the extinction coefficient in a cosmology independent way. Our precision based on this single system is only slightly weaker than constraints obtained analysing $\sim 10^3$ SNe in the Hubble-Lemaitre diagram. This can be improved with a number of sibling supernovae, and with different properties of the siblings, can also provide a cosmology independent constraint on both β and the lightcurve width-brightness correction factor, α. Thus, it is a complementary source of information for supernova cosmology, and can be also used to probe extinction in these systems even if a wide lever arm in wavelength range is missing.

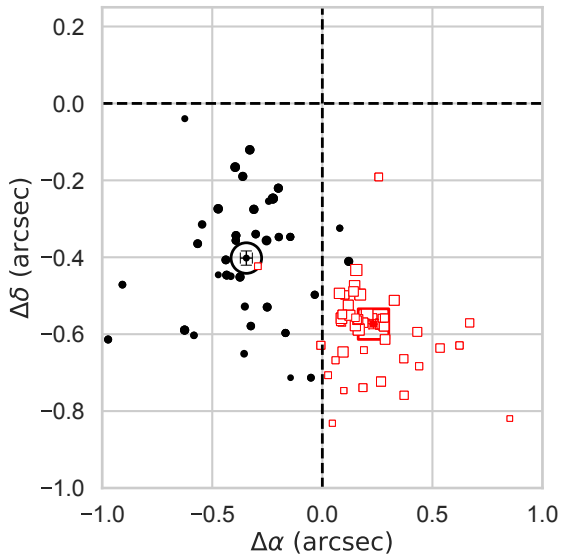

Figure 2. Positions of each alert corresponding to AT 2019lcj (filled black circles) and SN 2020aewj (open red squares) with the size of the markers proportional to the signal to noise ratio of the alert. The median positions of the alerts corresponding to each SN are highlighted using a large black open circle for AT 2019lcj , while the median position of alerts for SN 2020aewj is highlighted using a large open red square. The intersection of the two dashed lines shows the position of the host galaxy.

2 ZTF19aambfxc : THE TALE OF TWO SUPERNOVAE

The Zwicky Transient Facility (ZTF) survey is a 3π imaging survey of the Northern sky conducted on the (48-inch) Samuel Oschin Telescope at the Palomar Observatory (see Bellm et al. 2019b, for a more detailed description of the survey specifications) between 2018 and 2020, later replaced by ZTF-II. It included a public survey in g and r bands with a nominal $5-\sigma$ depth of ~ 20.5 mag with a 3-day cadence, along with a few programs run by the ZTF partnership including an extragalactic survey in the i-band with 4-day cadence, designed to obtain a three-filter lightcurve sample of Type Ia supernovae for cosmological applications. The procedure for processing the survey data and the data products are described in Masci et al. (2019). As part of the public survey, the Bright Transient Survey (BTS) (Fremling et al. 2020) is an effort aimed at collecting an untargeted, nearly complete, magnitude limited sample of spectroscopically classified transients reaching 18.5 mag.

ZTF19aambfxc (Nordin et al. 2019) is a transient detected on the core of a bright galaxy in the public 3-day cadence ZTF survey. It had detections in public alert photometry (SNR ≥ 5) from June 7 through August 14, 2019, and the i-band Partnership survey from June 11 and Aug 23, 2019, reaching a brightest observed magnitude of 18.69 in the r-band. After that, the transient faded below detection. ZTF19aambfxc was reported to TNS as AT 2019lcj. Since it never got as bright as 18.5 mag, the high completeness (93 %) threshold reported in the ZTF Bright Transient Survey Perley et al. (2020), it was, unsurprisingly, not followed up spectroscopically by BTS. Unfortunately, no independent spectroscopic classification has been reported either.

On January 27, 2020, i.e., about 200 days after the detection of AT 2019lcj, an apparent re-brightening of the source occurred, SN 2020aewj, shown in Fig. 1, reaching a significantly brighter state of 17.54 mag in g-band, well over the BTS classification threshold of 18.5 mag. Upon closer examination, the re-brightening was not at the exact same location as the first detection. The position of the ZTF19aambfxc alerts during this entire period are shown in Fig. 2, with the black markers denoting epochs before Julian Day 2458800 (Nov 12, 2019), while those after this date are shown in open red squares displaying the positional clustering of alerts during these phases. Visual inspection of the light curve for the alerts during these two time periods immediately made it evident that there were two distinct explosive transients with a small projected distance between them. While we do not show this light curve (built out of alerts) in the paper, this is also apparent from the forced photometry light curve shown in Fig. 3 discussed later in this section. The separation between the two transients as shown in Fig. 2, was $0.57''$. Consequently, these transients have been named AT 2019lcj and SN 2020aewj . At the time for the second event, the field was no longer part of the 4-day cadence Partnership i-band survey, thus the brighter SN was only observed in g and r-bands.

As part of BTS, the new transient, SN 2020aewj, was securely classified as a normal SN Ia, (Perley et al. 2021) using the Spectrograph for the Rapid Acquisition of Transients (SPRAT) (Piascik et al. 2014) on the Liverpool Telescope (Steele et al. 2004, henceforth LT). The LT spectrum is shown in Fig. 4, along with a spectrum of the "typical" normal SN Ia SN 2011fe at a similar phase. However, the older transient must be photometrically classified. We first describe the photometric light curves and then the host properties.

In the remainder of this section, we first discuss the association of a host galaxy with these two transients. This is followed by a description of the data processing steps needed to obtain a light

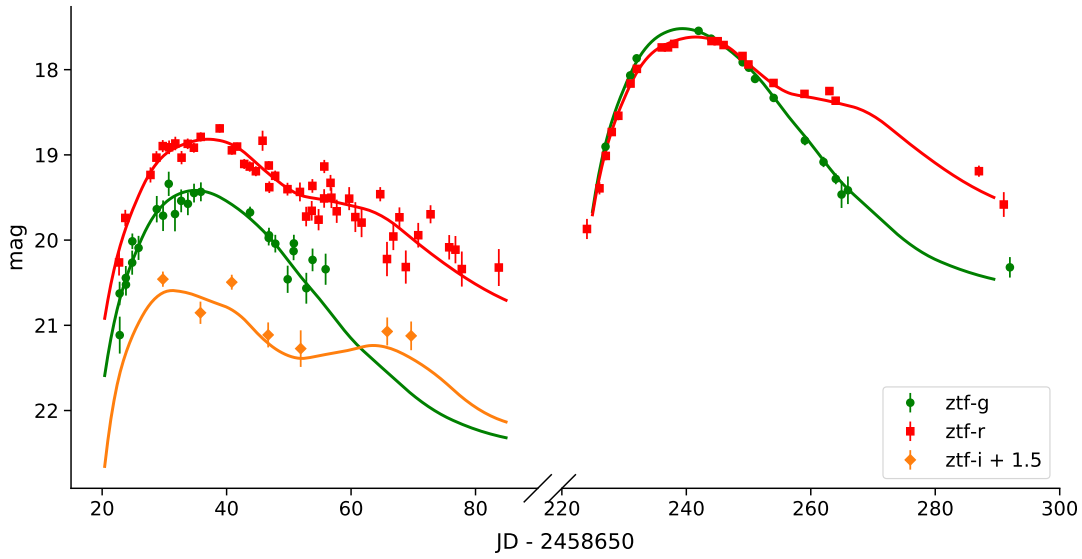

Figure 3. Observations of the sibling system at SNR > 3, in observed bands of the two individual supernovae where forced photometry at the location of AT 2019lcj after a Julian Day of 2458750 has been ignored, while early photometry at the position of SN 2020aewj has been ignored due to contamination. Along with the data, we show the best fit SALT2 model curves for each SN Ia . This shows the remarkable coincidence of having two SN Ia within the distance shown in Fig. 2 happen within ~ 200 days. The SALT2 parameters and uncertainties corresponding to the best fit model, and peak brightnesses in the ZTF filters are presented in Tab. 2, and are different by ~ 2 mag in the rest frame Bessell B-band.

Table 1. Positions of the two supernovae AT 2019lcj and SN 2020aewj separated by 0.57 ″ at z = 0.0541.

ID	RA (deg)	DEC (deg)	host sep (″)
AT 2019lcj	265.42935	67.96189	0.50
SN 2020aewj	265.42974	67.96183	0.42

curve and finally, we use both the host information and the light curves to classify the older transient.

2.1 Data Processing of the Transient Light Curves

Using the alert packet from the Growth Marshal (Kasliwal et al. 2019) associated with the transient ZTF19aambfxc, we split the observations into two groups assigning them to AT 2019lcj if the Julian Day of the observation, $JD \leq 2458800$ (Nov 12, 2019), and SN 2020aewj otherwise. The time of the split was determined by visual inspection. We determined the position of each SN, by taking the median of the positions of the 5σ detections for each SN. These locations are summarized in Table 1, and the positions of these detections are shown in Fig. 2.

We run forced photometry at these SN locations using a pipeline, hereafter known as the ZUDS pipeline[1] (Dhawan et al., in prep), which performs aperture photometry using the Astropy affiliated package PhotUtils (Bradley et al. 2019), using a six pixel diameter aperture on the difference images. The reference images for the difference images are constructed by co-adding exposures from epochs at least 30 days or more before the initial estimate of the time of maximum from the alert photometry, using the software SWARP (Bertin 2010). In order to build the co-add, we only take epochs with seeing between 1.7″ and 3″ and a magnitude limit deeper than 19.2 mag. For consistency, we use the same reference image for both SNe. In the ZUDS pipeline, difference images are obtained using HOTPANTS (Becker 2015), an implementation of the image subtraction algorithm (Alard & Lupton 1998). The zero points for each epoch are computed by IPAC, corrected for a six-pixel diameter aperture. For the *i*-band, we use the images corrected for an observed fringing pattern, using the fringez software (Medford et al. 2021). From the IPAC Forced Photometry Service (Masci et al. 2019) at the same locations, we obtain the metadata for each observation, including the magnitude limit $m_{\rm lim}$ of the observation, the seeing seeing of the observation and, the standard deviation $\sigma_{\rm pix}$ on the background at the pixel on which the SN is located. We combine this information with the ZUDS pipeline results for data quality assessment. Specifically, we only use those observations that satisfy the following conditions: $1.0'' < \text{seeing} < 4.0''$, $m_{\rm lim} < 19.2$ mag, $\sigma_{\rm pix} < 14.0$, where $\sigma_{\rm pix}$ is the robust sigma per pixel in the science image and is used as a metric to remove non-photometric data. We then use a maximum-likelihood method to fit the SALT2 model to each of these two supernova light-curves. The low seeing values are removed to protect against undersampling during image subtraction. We then remove the epochs that have $5-\sigma$ flux outliers relative to the best fit SALT2 model (discussed later and summarized in Tab. 2) and use the remaining selected points as the light curves of the individual supernovae. The final photometry datasets used are included as Tables C and C2. The resulting light curves are shown in Fig. 3. As stated earlier, this light curve clearly shows the presence of two transients with no detections for a period of over 100 days in between. For the unclassified transient AT 2019lcj , we notice

[1] https://github.com/zuds-survey/zuds-pipeline

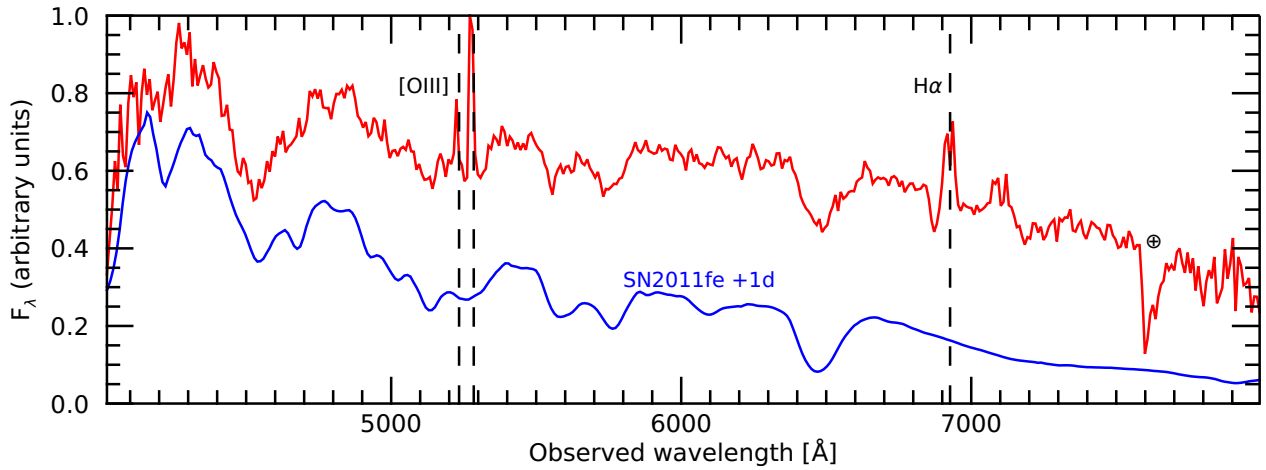

Figure 4. Spectrum of SN 2020aewj obtained at on 2020-02-17 with the Liverpool Telescope. The spectrum was classified as a SN Ia in the TNS classification report (Perley et al. 2021) and provides an approximate redshift of ∼ 0.055 for the supernova. A comparison with a spectrum from SN 2011fe at the same epoch from a compilation by Amanullah et al. (2014) is shown. A more accurate host galaxy redshift, $z = 0.0541$, was measured based on the [OIII] and H_α lines, primarily using a spectrum from NOT, obtained more than two months later when the SN had faded.

Table 2. Properties of the two SNe AT 2019lcj and SN 2020aewj: The `SALT2` parameters of the SNe based on a maximum likelihood fit, along with the synthetic peak magnitudes for this best fit model in the ZTF g-band, r-band and i-band along with the Bessell B-band.

ID	t_0 (day)	$10^4 \times x_0$	x_1	c	g peak (mags)	r peak (mags)	i peak (mags)	B peak (mags)
AT 2019lcj	2458685.41 ± 0.15	2.67 ± 0.12	0.54 ± 0.18	0.57 ± 0.04	19.4	18.8	19.1	19.7
SN 2020aewj	2458889.92 ± 0.08	17.08 ± 0.56	0.61 ± 0.13	0.00 ± 0.03	17.5	17.6	18.2	17.6

that AT 2019lcj has a shoulder in the redder bands ($r-$band and $i-$band) as seen in Fig. 3 strongly indicating that the SN is of Type Ia. We will verify this shortly after discussing its redshifts and host properties.

Host Association and Properties: The top panel of Fig. 5 shows the positions of the supernovae and the two nearest galaxies. Both supernovae are found to lie on the core of a galaxy, while there is a second nearby galaxy, approximately 30″ away which we deem extremely unlikely to be the host of any of the two SNe. We will refer to the first galaxy as the host galaxy. A high SNR spectrum from the ALFOSC instrument on the Nordic Optical Telescope (NOT) [2] taken on April 28, 2020 was used to determine the properties of the galaxy. The host galaxy redshift was accurately measured to be $z = 0.0541$ from the position of [OIII] and Hα lines, in excellent agreement with the best fit to the SN spectrum of SN 2020aewj ∼ 0.055. This late spectrum is available from the authors upon request. The angular distances along with the absence of a nearby galaxy establishes the two transients as siblings, i.e. have the same host galaxy. Additionally, the spectrum from the host provides us with an accurate measurement of their common redshift, used in the calculations later.

While the two conclusions above are central to this paper, we expand our study of the properties of the host galaxy as it might be relevant to the conclusions on extinction. We retrieve the science-ready co-added images from the Sloan Digital Sky Survey data release 9 (SDSS DR 9; Ahn et al. 2012), the Panoramic Survey Telescope and Rapid Response System (Pan-STARRS, PS1) DR1 (Chambers et al. 2016), the Two Micron All Sky Survey (2MASS; Skrutskie et al. 2006), and preprocessed `WISE` images (Wright et al. 2010) from the unWISE archive (Lang 2014)[3]. The unWISE images are based on the public `WISE` data and include images from the ongoing NEOWISE-Reactivation mission R3 (Mainzer et al. 2014; Meisner et al. 2017). We use the software package LAMBDAR (Lambda Adaptive Multi-Band Deblending Algorithm in R) (Wright et al. 2016), which is based on a software package written by Bourne et al. (2012) and tools presented in Schulze et al. (2020), to measure the brightness of the host galaxy. The spectral energy distribution (SED) was modelled with the software package Prospector[4] version 0.3 (Leja et al. 2017). We assumed a linear-exponential star-formation history, the Chabrier (2003) IMF, the Calzetti et al. (2000) attenuation model, and the Byler et al. (2017) model for the ionized gas contribution. The priors were set as described in Schulze et al. (2020).

The best fit host galaxy SED, along with its parameters, is shown in the lower panel of Fig. 5. This shows that the stellar mass of the galaxy is $\sim 10^{10.48^{+0.11}_{-0.46}} M_\odot$. This is approximately equal to the threshold usually chosen to divide SN Ia samples into two groups to which different corrections are applied. Fortunately, this will not have an impact on our calculations which depend on the difference of the distance moduli of the pair as the pair share the same host galaxy. We also note that the measured stellar mass is very comparable to the Milky-Way value reported by Licquia &

[2] PI: Sollerman & Goobar

[3] http://unwise.me

[4] https://github.com/bd-j/prospector

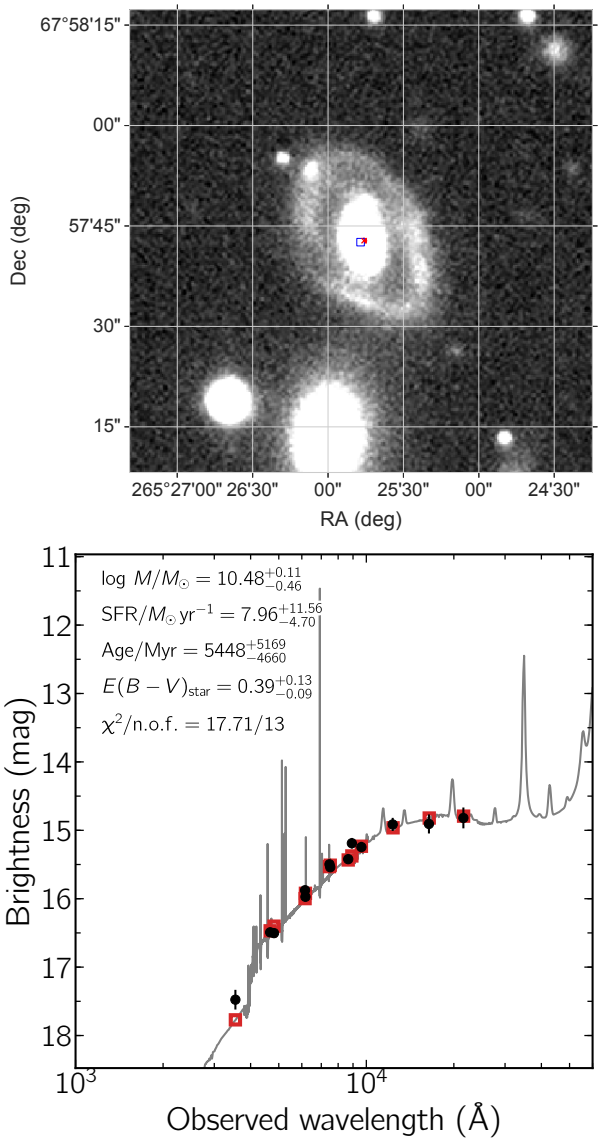

Figure 5. Host association and Properties: (Top panel) Location of nearby galaxies obtained from the Legacy Survey in g band from the NOAO data lab is shown in a red cross, while SN 2020aewj is shown with a blue open square almost spatially coincident in the core of the host galaxy (Bottom Panel) The best fit model spectral energy distribution of the host galaxy of ZTF19aambfxc (photometric observations •, model-predicted magnitudes □) from multi-band photometry. The solid line displays the best-fitting model of the SED. The fitting parameters are shown in the upper-left corner. The abbreviation n.o.f. stands for numbers of filters.

Newman (2015), thus the dust properties of this host galaxy are expected to be similar to the Milky Way, even in a model like Brout & Scolnic (2021).

Photometric Classification of the AT 2019lcj : To verify the SN Ia class suspected from the light curve shape, we evaluate the maximum likelihood fit to to the lightcurve in Fig. 3 with models of different supernova classes and sub-types. Since the models considered have different numbers of parameters and are non-nested, we cannot use the likelihood ratio test. Rather than computing the Bayesian evidence for each model which is computationally expensive, and the population priors are likely not well known, we use the Bayesian Information Criteria (BIC) (Schwarz 1978) for each model, which for Gaussian distributed deviations amounts to

Table 3. Bayesian Information Criterion of different SN types fitted to the multi-band photometry of AT 2019lcj shown in Fig. 3.

SN type	BIC	ΔBIC
SN Ia: Norm	419.47	0.
SN Ia: 91bg	1200.22	780.75
SN Ibc	1042.55	623.08

$$\mathrm{BIC} = -2\log(L_{\max}) + k\log(n) \quad (1)$$

where $L_{\max}$ is the maximum of the log likelihood, n is the number of data points and k is the number of parameters in the model. The difference in BIC values between two models is approximately proportional to the logarithm of the Bayes ratio of the two models, with $\Delta BIC = 10$ considered decisive evidence against the model with higher BIC (Liddle 2007). Applying a maximum likelihood fit to different kinds of templates of supernovae types, we calculate the BIC values as shown in Table 3. We choose the SN Ib/c template kindly provided Peter Nugent [5] and the K-correction estimates in Nugent et al. (2002). Since the observed colours of the SN are red, we also fit the SN1991bg template from Nugent et al. (2002). The column ΔBIC has values of BIC$(model) - BIC(\texttt{SALT2})$. Thus models considered here with $\Delta BIC >> 10$ are decisively disfavoured. Thus, the entries in Table 3 show that from the photometric data alone, we can say that of the types of supernovae and templates considered, AT 2019lcj is a Normal SN Ia .

3 METHOD

Sibling supernovae are inferred to be in the same galaxy through their transverse proximity, and thus have virtually identical (radial) distance. First, we quantify the potential difference in the radial distance in comparison to the intrinsic dispersion of SN Ia. Galaxies are typically of size ∼ kpc , and host SN Ia within a few tens of kpc from the centre of the galaxy (Galbany et al. 2012; Gagliano et al. 2021). Thus, sibling supernovae are expected to have a distance difference $\delta d \lesssim 100$ kpc , resulting in a distance modulus difference of $5/\ln(10) \times \frac{\delta d}{d}$. For a sibling at a redshift of $z = 0.0541$, even for a distance difference of ∼ 100 kpc this difference is $\approx 10^{-3}$ which is two orders of magnitude smaller than the distance uncertainty induced by the intrinsic dispersion of $\sigma_{int} \sim 0.1$ of SN Ia . This understanding can be expressed as a prior probability which is a normal distribution in the difference of the distance moduli with a standard deviation related to the intrinsic dispersion

$$\mathcal{N}(\Delta\mu, \sigma^2). \quad (2)$$

In this work, we assume the SALT2 model with an intrinsic dispersion affecting the brightness of SN Ia coherently at all wavelengths (technically following the G10 intrinsic dispersion). This means that the estimated distance modulus of a supernova can be normally distributed about the true distance modulus with a standard deviation of σ_{int}. The value of the intrinsic dispersion in supernova samples is determined for each sample, and is generally ∼ 0.1 mag . The intrinsic dispersion of SN Ia in the same galaxy (or equivalently if sibling supernovae have correlated intrinsic scatter)

[5] https://c3.lbl.gov/nugent/nugent_templates.html

has been investigated (Scolnic et al. 2020; Burns et al. 2020) and found to be consistent with low correlations r. Thus, we choose the standard deviation in our prior probability to be $\sigma^2 = 2\sigma_{int}^2(1-r)$, with a fiducial value of $r = 0$. We also use the Tripp relation (Tripp & Branch 1999) as used in recent supernova cosmology analyses (Brout et al. 2019; Hinton et al. 2019; Scolnic et al. 2018; Jones et al. 2018a; Betoule et al. 2014)

$$\mu_i = m^{\star}_{B\ i} + \alpha \cdot x_{1i} - \beta \cdot c_i - M^{\star}_{Bi} + \delta_{\mathrm{Host_i,loc_i}}\mu, \quad (3)$$

where, for completeness, we have included a correction term for (potentially local) environment dependence. The term involving the impact of the host galaxy has been mostly used in the supernova cosmology literature as a step function involving the global properties of the host galaxy such as stellar mass $M^{\mathrm{Host}}_{\mathrm{stellar}}$, as in $\delta_{\mathrm{Host,loc}}\mu = \mathrm{step} \times (M^{\mathrm{Host}}_{\mathrm{stellar}} - M_{\mathrm{thresh}})$ where step ~ 0.1 mag and $M_{\mathrm{thresh}} \sim 1 \times 10^{10} M_{\odot}$ are obtained by minimizing the Hubble residuals from a fiducial model. For such a model where the environmental dependence is through global properties of the host, clearly this difference disappears for supernova siblings. However, such environmental dependence is expected to depend on the local properties of the galaxy. For example, this may be driven by the properties of the progenitor(s) which inherited the properties of the local stellar population or due to dust which could also be local. This could have important consequences for the measurements of H_0 (Rigault et al. 2015, 2020), though the details are part of a current debate (Jones et al. 2018b). Thus, these siblings, even though separated by a tiny projected distance, could be further apart in the galaxy (radially) and have different properties. Nevertheless, as far as estimated corrections go, corrections from local properties are made by analyses restricted by projected distances, often in regions of projected distances of $\sim$ 2 kpc. The siblings being 0.57 kpc apart are close enough that any correction term due to local measurements would also be extremely similar for the two SNe Ia and thus the difference would be small. Thus, we set $\delta_{\mathrm{Host,loc}}$ to 0 in the rest of this work.

Thus, for a pair of sibling supernovae, we get

$$\Delta\mu \equiv \mu_1 - \mu_2 = -2.5 \log (x_{01}/x_{02}) + \alpha \cdot (x_{11} - x_{12}) - \beta \cdot (c_1 - c_2) \quad (4)$$

where we have used the approximation $m^{\star}_B = -2.5 \times \log 10(x_0) + K$, where K is a constant.

In this model, the parameters are $\Psi = \{\psi, \phi_1, \phi_2\}$, where the SALT2 model parameters for each supernova are $\phi \equiv \{x_0,\ x_1,\ c\}$, and the subscripts 1 and 2 refer to the two supernovae, and $\psi \equiv \{\alpha, \beta\}$. We can write the posterior distribution $P(\Psi|D, \mathcal{H})$ on Ψ where D is the photometric data, along with spectroscopic data needed to determine the redshift z, and $\mathcal{H}$ represents our understanding of the astrophysics leading to the equations we use:

$$\begin{aligned} P(\Psi|D,\mathcal{H}) &\propto P(D|\Psi,\mathcal{H})\Pi(\Psi|\mathcal{H}) \\ &= P(d_1|\phi_1,\mathcal{H})P(d_2|\phi_2,\mathcal{H})\Pi(\Psi|\mathcal{H}) \\ \Pi(\Psi|\mathcal{H}) &= (\mathcal{N}(\mu_1 - \mu_2, \sigma^2)\Pi(\alpha)\Pi(\{\beta, \phi_1\ \phi_2\}), \end{aligned} \quad (5)$$

where $P(D|\Psi, \mathcal{H})$ is the likelihood function of Ψ, and $\Pi(\Psi|\mathcal{H})$ is the prior on Ψ. Utilizing the fact that the time of peak of the supernovae are reasonably well constrained, and the flux due of AT 2019lcj is negligible at the time of SN 2020aewj which peaks 205 days after AT 2019lcj , factorizing the likelihood function into independent likelihood functions for the data of AT 2019lcj and SN 2020aewj is an excellent approximation. Therefore, we write this as the product of individual likelihood functions $P(d_i|\phi_i, \mathcal{H})$ is the likelihood function of the SALT2 model parameters for the ith supernova. These functions encode the assumption that the measured fluxes are Gaussian distributed about the SALT2 model fluxes with variances described by the flux uncertainties reported in the photometry, as well as the uncertainties on the model as determined from SALT2 training. The prior $\Pi(\Psi|\mathcal{H})$ includes chosen priors on each of the parameters $\Pi(\alpha)\Pi(\beta\ \phi_1\ \phi_2)$. Our chosen priors on each parameter in Ψ in this paper are un-informative (uniform, hard priors) except for α for which we sometimes adopt the Pantheon result (Scolnic et al. 2018), as described as part of each calculation in Sec. 4. Aside from these choices, we use the result of a different measurement (galaxy association) affirming that these SN Ia are siblings, to further constrain these parameters, expressed as the normal distribution Eqn. 2 using Eqn. 4 for $\Delta\mu$. We use `emcee` (Foreman-Mackey et al. 2013) to explore the parameter space.

4 RESULTS

Constraints on β: Having confirmed that the siblings are SNe Ia we employ the methodology discussed in Sec. 3 to calculate the posterior distribution of all the parameters Ψ based on the data from the siblings in Fig. 6. We take into account the spatial coincidence of this sibling pair, thereby using Eqn. 4 and calculate the posteriors using Eqn. 5. In Fig. 6, the blue contours enclose 68% and 95% of the probability while the dashed black lines show the maximum likelihood estimates of the parameters from each of the single supernovae. Uninformative uniform box priors were used as hard priors on all of the parameters except α where a Gaussian prior of 0.15 ± 0.01 incorporating the values obtained in the analysis of the Pantheon data set (Scolnic et al. 2018) were used. The constraints on the parameter α effectively stems entirely from the Pantheon prior. The excellent match between the maximumlikelihood estimates of the individual supernovae in Tab. 2 (with no knowledge of the sibling nature) and the posteriors of the joint likelihood confirm the expected result that SALT2 parameters of individual supernovae are not affected by the global parameters like α and β. Thus, the only new information from the sibling nature is the constraints on β which would be entirely unconstrained from the individual fits of two supernovae.

Consistency of β constraints with previously reported values: Therefore, we focus on the constraints on β from this system. In Fig. 7, we show the posterior probability density function on β inferred from the sibling supernova system, when marginalized over all other parameters in Ψ, and using the Pantheon prior on α. The constraints are 3.5 ± 0.3 which is a 8% measurement on the parameter β from this system alone. This can be compared to constraints on β from cosmological surveys, in terms of consistency of values summarized in Tab. 2 and the magnitude of uncertainty. Supernova cosmology survey results in the past decade using the SALT2 model include the Joint Light Curve Analysis (JLA), the results on the Pantheon sample from PanSTARRS and the Dark Energy Survey. All of these surveys presented results with the G10 and the C11 intrinsic scatter models. Of these the JLA studied the constraints on α, β based on different cosmological models, and the use of complementary information from Cosmic Microwave Background and galaxy surveys, while the other studies presented cosmological model insensitive constraints using `SALT2mu`. For the G10 scatter model, JLA reported values of β between $3.099 - 3.126$ with an uncertainty of $\sim 0.075 - 0.1$

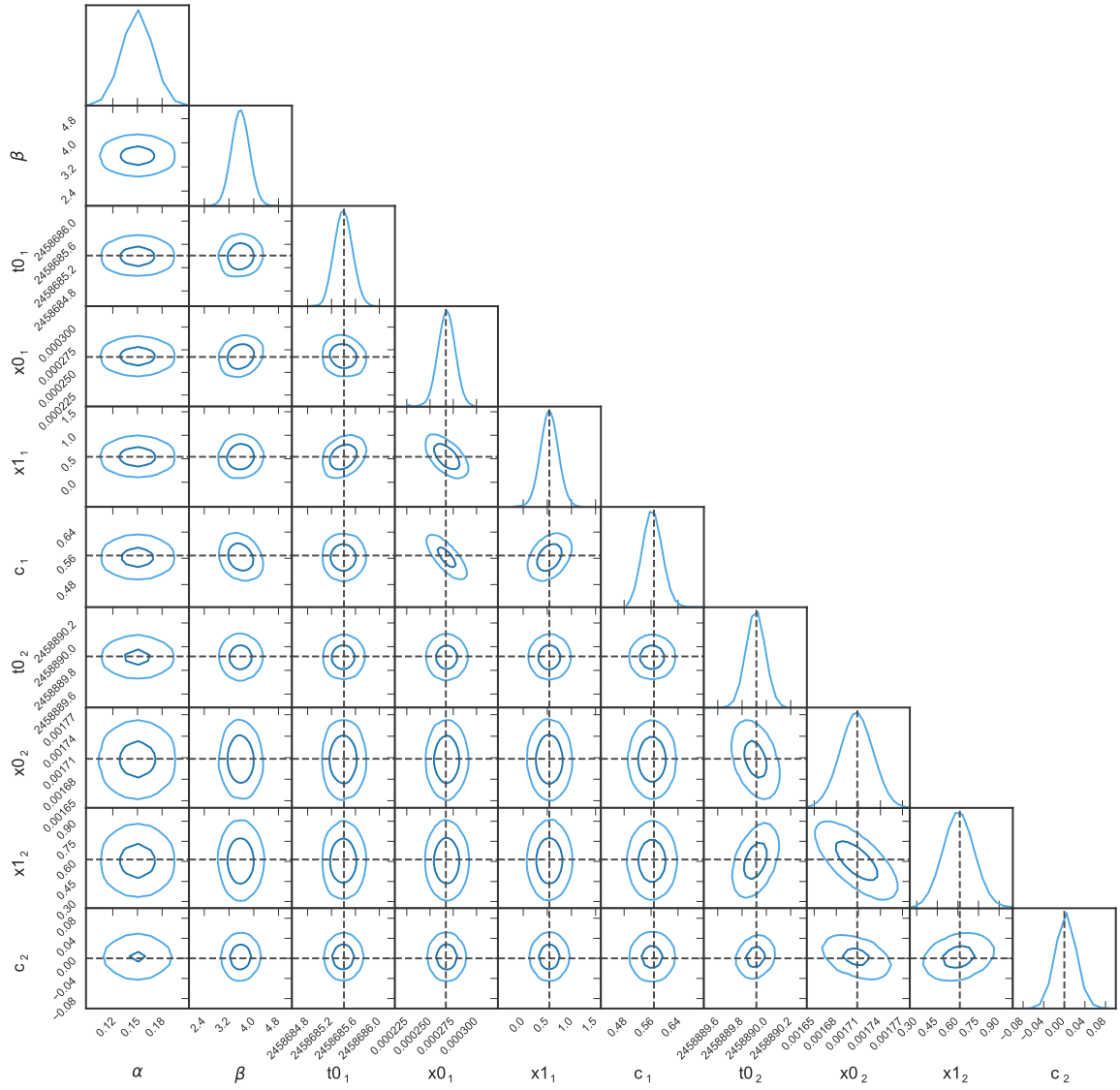

Figure 6. The joint posterior distribution of the SALT2 light curve parameters for the two supernovae and the global parameters α and β. The contours enclose 68% and 95% of the probability while the dashed lines show the maximum likelihood estimates of the parameters shown in Tab. 2 if available from each of the single supernovae. Uninformative uniform box priors were used as hard priors on all of the parameters except α where a Gaussian prior of 0.15 ± 0.01 was used incorporating the values obtained in the analysis of the Pantheon data set (Scolnic et al. 2018).

while the DES/PanSTARRS analysis obtains a slightly lower value $3.02 - 3.03$ with an uncertainty of $\sim 0.11 - 0.13$. The values with a C11 intrinsic scatter model based on the SNFactory studies are consistently higher, ranging from $3.27 - 3.4$ with a similar uncertainty ~ 0.1 while the values obtained from DES and PanSTARRS range from $3.51 - 3.61$ with the uncertainties of the order $0.15 - 0.25$. Clearly the values here are very consistent with C11 intrinsic scatter model values reported from past surveys, while the the consistency with G10 scatter model based analyses is at the level of $< 2\sigma$. Finally, we show the comparison with a determination of β from 69 low redshift SN Ia (Dettman et al. 2021) from the Foundation Supernova Survey (Foley et al. 2018).

Impact of Priors and Assumptions: In this work, we do

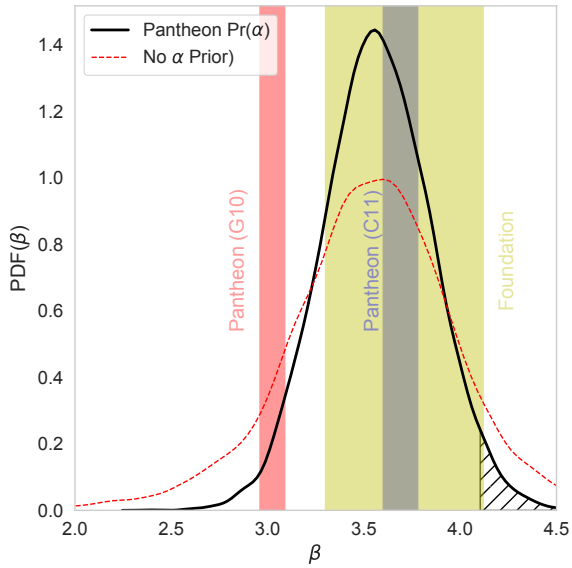

Figure 7. The PDF of β marginalized over all other model parameters is shown in solid (dashed) black (red) curve for an intrinsic scatter of 0.1 and correlation r=0, with (without) the Pantheon priors on α. The constraints are $\beta = 3.4(3.6) \pm 0.3$ (0.4). The shaded vertical rectangles show the $1-\sigma$ constraint on β from the PanSTARRS spectroscopic sample (Scolnic et al. 2018) for the G10 model of intrinsic scatter (red) and the C11 model (blue) and for 69 low redshift SN Ia from the Foundation Supernova Survey (yellow) (Dettman et al. 2021). The hatched red region shows the probability of the β value being at least as large as the value expected if the colour dependent extinction was solely due to ISM host dust of the same nature as the Milky Way. This probability associated with this region is 2.5 %.

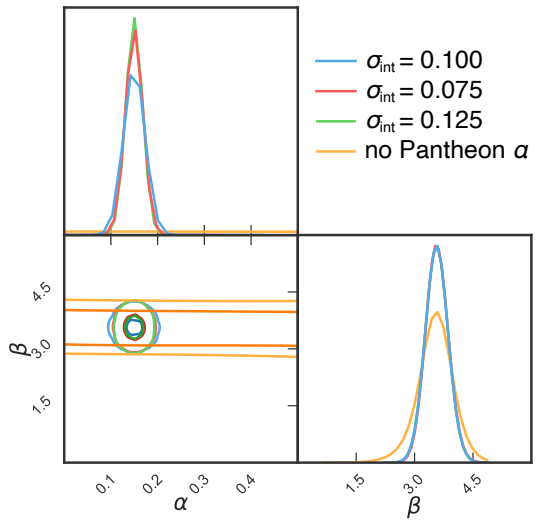

Figure 8. Joint Constraints on α and β from the SN Ia sibling system when the magnitude of intrinsic dispersion used in calculating the posterior is varied from the fiducial value of 0.1 (blue) to 0.075 (red) and 0.125 (green). Finally, the orange contours show the results for the fiducial choice of $\sigma_{int} = 0.1$ when the Pantheon priors on α are not used. This leaves α completely unconstrained. but the constraints on β only change slightly from 3.4 ± 0.3 to 3.6 ± 0.44

not estimate the intrinsic dispersion as is customary in supernova cosmology analysis. Instead, we posit that the magnitude of intrinsic dispersion is 0.1 based on results from previous surveys. Therefore, in Fig. 8, we study the impact of constraints on α and β as we vary the magnitude of the intrinsic dispersion. Fig. 8 shows the constraints on α and β for the fiducial case (shown in Fig. 6) of $\sigma_{int} = 0.1$ (blue) and two additional cases: $\sigma_{int} = 0.075$ (red) and $\sigma_{int} = 0.125$ (green). Within this small range of changes to the assumed values of intrinsic dispersion, the constraints on β are unaffected. Finally, this figure also explores the impact of not using the Pantheon data set to put a prior on α (orange). We find that removing this prior leaves α entirely unconstrained but the constraints on β only change modestly from $\beta = 3.4 \pm 0.3$ to 3.6 ± 0.4. We can understand this insensitivity as arising from the peculiarities of the sibling system: The x_1 values of the two SN Ia have virtually the same value, while the difference in c is large. This leads to a very tiny dependence on α in Eqn. 4, and consequently has small effects on the constraints on β. The downside of this same peculiarity is that without priors, the constraints on α are extremely weak as shown in Fig. 8.

Comparison with Milky Way R_B: Data driven models like `SALT2` do not require any physical interpretation to parameters like β, but as a best fitted value to the Tripp relation for a sample of SNe Ia. However, the colour excess (after correction for Milky Way reddening) is interpreted in other models (see for example, Tripp & Branch (1999)) as dust-extinction in the host galaxy and is described by a fitting function dependent on the total-to-selective extinction ratio R_V (Cardelli et al. 1989), or in the restframe B-band, $R_B = R_V + 1$. In such models, one cannot exclude different values of R_V in each galaxy, describing the size and composition of the dust-grain population in the host galaxy ISM along the line-of-sight. Such a measurement of R_V in diverse populations of galaxies is poorly known, but is well measured in the Milky Way, where it varies with direction and has an average value of $R_V = 3.1$. Using the Tripp (1998) relation, one may expect that the value β is related to the R_V for extinction as $\beta \approx R_B$. Therefore supernova surveys (as discussed above) usually obtain values of β consistent with $R_V \approx 2$, well below the average Galactic value, but cannot probe the distribution or variance of R_V. This can be done using longer lever arms in colour (see e.g. Amanullah et al. 2015, and references therein). In this work we show that one can also extract it from galaxies that host supernova siblings, as the β value inferred here is specific to the host galaxy. The R_V value implied by our constraints is similar ~ 2.5, and the probability of the implied R_V value being at least as large as the average Milky Way value has a total associated probability of 2.5%. We note, however, that deviations from the "standard" dust law have also been reported in Galactic studies (see e.g., Nataf et al. 2016).

Since this determination of R_V is model dependent, we study this in other models as well. First, as a consistency check, we also compute the total-to-selective absorption ratio, R_V, using the SN Ia model in `SNooPy` (Burns et al. 2011). `SNooPy` fits the host galaxy R_V and colour excess, $E(B-V)$ using templates based on the colour-stretch parameter, S_{BV} (Burns et al. 2014). We present details of the inference procedure in Appendix A, but summarize the results $R_V \sim 2.8$. Finally, we also look at the more general dust model from Brout & Scolnic (2021) in Appendix B. In this model, the colour of a SN Ia as determined by `SALT2` is postulated

to be a linear combination of reddening due to to dust in the host galaxy, and colour of the supernova with respect to a template with coefficients R_B and β. Thus, there are two colour laws in this model, and more free parameters compared to the traditional SALT2 model. The parameter β in this model is not directly related to R_B. While we postpone a more complete uncertainty analysis to future work, we show that the sibling system can be used to probe such models. For example, it suggests that if R_V is 3.1 (the host galaxy of these siblings has a similar stellar mass as the Milky Way), we can show that this suggest a difference in c_{int} of $\gtrsim 3$, which is much larger than the standard deviation of the Gaussian distribution for individual SN, which is ameliorated for a lower R_V and low values of β. Therefore, in multiple models, this sibling pair suggests that the host galaxy has a lower value of R_V than the Milky Way.

Uncertainty and Future Prospects: As discussed earlier, the uncertainty on β obtained from cosmological surveys in the last decade depend on the intrinsic scatter model used, and range from $0.075 - 0.15$ for the G10 model, and $0.15 - 0.25$ using the C11 model. These surveys use a large number of SN Ia for example 740 in JLA, 207 in DES, 1048 in the Pantheon Sample, 1364 in the photometric PanSTARRS analysis to obtain such constraints and are tighter by the constraints from this single system by a factor of $2 - 3$. For constraints from sibling supernovae to be useful in understanding distance modulus bias, it is important for these constraints to be competitive, which is possible by combining the results from a number of SN Ia siblings. Currently, ZTF has a few SN Ia siblings (see Graham et al., 2021, in prep), while data collection continues in phase II. DES has published a few siblings, and one can expect more siblings from large ongoing surveys like ZTF, Young Supernova Experiment (Jones et al. 2021) and upcoming surveys like the Legacy Survey of Space and Time (LSST Science Collaboration et al. 2009; Ivezić et al. 2019) at the Vera C. Rubin Observatory. While a simple square root of N calculation would suggest that ~ 10 sibling systems should tighten the constraints to competitive levels, this actually depends on the properties of the SN Ia themselves.

5 DISCUSSION

The key properties of the observations we have used is that the siblings share both the same exact line of sight, i.e., avoiding any potential differential contribution from Galactic extinction. Furthermore, they were measured with the same instrument and reference images, further reducing potential systematic uncertainties. We have exploited the fact that the distance moduli of two supernovae in the same galaxy are virtually identical and any radial difference is much smaller than the impact from intrinsic dispersion. We quantify this at the beginning of Sec. 4. This property is also the principle used to transfer distance measurements from other calibrators in building the local distance ladder. This is insensitive to peculiar velocities of the host galaxy because we do not use the cosmological distances as function of the redshift through a cosmological model. The only way peculiar velocities enter our calculation is through K-corrections required to transform from the observed frame with the spectroscopic redshift of the host galaxy (which combines the impact of cosmological redshift and peculiar velocities) to the rest frame of the SN Ia and is known to be tiny for typical or fairly extreme peculiar velocities. In any case, since this uncertainty is shared by both SNe, it nearly cancels. While this pair of siblings is in the Hubble flow, this means that even the lowest redshift siblings found in the future that might not be in the Hubble flow can be used in analyses like this. While an often discussed issue with with such distance ladder measurements in the impact of the environment through local and global properties of the host galaxy, such correction terms based on local properties have no impact in our particular example, as discussed in Sec. 4 due to the coincidental projected proximity of the two SN Ia. For more generic cases of SN Ia siblings, we are unlikely to repeat such proximity, and differences in SN Ia distances might need to take into account the differences in local stellar populations. While that would complicate the computation we did for other cases, this could also potentially help in resolving the difference between local and global dependence on galaxy properties.

The strength of our constraints on β and the relative insensitivity on α stems from the difference in light curve parameters of the SN Ia siblings we have chosen. These SN Ia have virtually the same light curve shape parameter x_1 while their colour parameter c are different by about 0.6 mag. However, we should note that SN Ia that are so red are usually removed from cosmological samples, which often put a constraint $|c| < 0.3$, and that the SALT2 training samples do not have such red supernovae.

6 CONCLUSIONS

Standardization of SN Ia and the characterization of systematic uncertainties in the process remains a crucial piece of supernova cosmology and its application to constraining the phenomenology of dark energy and the Hubble tension. Such systematics are particularly important when using supernova samples promised by ongoing and upcoming surveys where the large supernova sample size is expected to reduce the statistical uncertainties. Within the current industry standard of standardization based on the SALT2 model, an important aspect is the determination of population level parameter α, β that determine the linear importance of light curve shape and colour of SN Ia relative to their observed brightness in the standardization process. In the conventional process, this determination of α, β can depend on the cosmological models used, the contribution due to environmental effects, and the Malmquist bias of the survey sample relative to the training sample. The estimates are often corrected for using catalogue simulations that forward model entire surveys and their selection function using input populations of SN Ia that are inferred from data. This is a complex process. Hence complementary and independent information determining these parameters would be extremely useful.

In this work, we use the key property of siblings that the difference in distances of sibling supernovae are tiny and a few orders of magnitude below the intrinsic dispersion of supernovae. Since the difference of sibling distances are thus independent of cosmology or environmental properties, we introduced a method using a pair of sibling SN Ia (i.e. hosted in the same galaxy) obtained from the ZTF survey, to constrain the parameter β to 3.5 ± 0.3. While the historically reported values of β have been much lower, their values have stabilized for the past few years. Our reported values are consistent with the latest literature global values assuming a single β for all SNe, but has a precision which is somewhat worse than the

current state-of-art. Its advantage is that it is independent of several of the systematic uncertainties of the current methodology. For example, this does not depend on how accurately the population of SN Ia has been modeled in simulations, or how accurately the simulations can represent complex time domain surveys. While we demonstrate this method with a particular pair of siblings, where the constraints on β was expected to be strong (due to the differences in the best fit values of the SN Ia model parameters), the method can be extended to samples of siblings. This would not have been easy in the past, as sibling SN Ia are rare. Thanks to the dramatic improvement in sky survey volume, ongoing surveys are reporting several SN Ia siblings. As we continue to wide-field surveys like ZTF Phase II, Young Supernova Experiment (YSE) and the Large Synoptic Survey Telescope (LSST) on the Vera C. Rubin Observatory, sibling SN Ia will be much more commonly found, allowing this method to be applied to a sample for accurate tests of the SN Ia] standardization needed for precision cosmology. If the sample contains siblings whose light curve shape parameters differ significantly as well, this method can constrain both α, and β without other priors. Significant work has gone into developing standardization models (see e.g. Saunders et al. 2018; Léget et al. 2020; Hayden et al. 2019), that are expected to improve upon `SALT2`. Such models involve different (and more) free parameters that need to be determined in a manner similar α and β in the `SALT2` model. Presumably, this method can be applied in a similar way, though we have not tried this at all.

A different path to better standardization is improving our understanding of the physical processes underlying the success. One of the most promising routes has been interpreting the physics underlying the colour dependent term standardization. This could be attributed to intrinsic colour diversity of SN Ia and physics connecting this to the brightness, or/and extinction due to dust in the interstellar medium of the host galaxy, and possibly in the circumstellar environment. Studies for this have used statistical sub-samples of SN Ia based on hosts, or samples of individual SN Ia where the extinction parameters are determined through measurements at multiple wavelengths, including space observations in the near-UV (see e.g. Amanullah et al. 2015), or even into the mid-IR (Johansson et al. 2017). Again using the independence of distance/brightness differences of SN Ia in the same galaxy, sibling SN Ia promise an alternative way of probing extinction through accurate measurements of attenuation with well-calibrated systems.

7 ACKNOWLEDGEMENTS

RB was supported by the research project grant "Understanding the Dynamic Universe" funded by the Knut and Alice Wallenberg Foundation under Dnr KAW 2018.0067. AG acknowledges support from the Swedish Research Council under Dnr VR 2016-03274 and 2020-03444. SD acknowledges support from the Isaac Newton Trust and the Kavli Foundation through Newton-Kavli fellowship. MR, MS and YLK have received funding from the European Research Council (ERC) under the European Union's Horizon 2020 research and innovation programme (grant agreement n°759194 - USNAC). ECK acknowledges support from the G.R.E.A.T research environment funded by *Vetenskapsrådet*, the Swedish Research Council, under project number 2016-06012, and support from The Wenner-Gren Foundations.

Based on observations obtained with the Samuel Oschin Telescope 48-inch and the 60-inch Telescope at the Palomar Observatory as part of the Zwicky Transient Facility project. ZTF is supported by the National Science Foundation under Grant No. AST-1440341 and a collaboration including Caltech, IPAC, the Weizmann Institute for Science, the Oskar Klein Center at Stockholm University, the University of Maryland, the University of Washington, Deutsches Elektronen-Synchrotron and Humboldt University, Los Alamos National Laboratories, the TANGO Consortium of Taiwan, the University of Wisconsin at Milwaukee, and Lawrence Berkeley National Laboratories. Operations are conducted by COO, IPAC, and UW.

The ZTF forced-photometry service was funded under the Heising-Simons Foundation grant. This work was supported by the GROWTH project funded by the National Science Foundation under Grant No 1545949. Based on observations obtained with the Samuel Oschin Telescope 48-inch and the 60-inch Telescope at the Palomar Observatory as part of the Zwicky Transient Facility project. ZTF is supported by the National Science Foundation under Grant No. AST-2034437 and a collaboration including Caltech, IPAC, the Weizmann Institute for Science, the Oskar Klein Centre at Stockholm University, the University of Maryland, Deutsches Elektronen-Synchrotron and Humboldt University, the TANGO Consortium of Taiwan, the University of Wisconsin at Milwaukee, Trinity College Dublin, Lawrence Livermore National Laboratories, and IN2P3, France. Operations are conducted by COO, IPAC, and UW.

Based on observations made with the Nordic Optical Telescope, operated by the Nordic Optical Telescope Scientific Association at the Observatorio del Roque de los Muchachos, La Palma, Spain, of the Instituto de Astrofisica de Canarias.

software: Numpy (van der Walt et al. 2011), Astropy (Astropy Collaboration et al. 2013, 2018), sncosmo (Barbary et al. 2016), PhotUtils (Bradley et al. 2019), ZTFQuery (Rigault 2018), SWARP (Bertin 2010), HOTPANTS (Becker 2015), ZUDS, fringez (Medford et al. 2021), LAMBDAR Wright et al. (2016), Prospector (Leja et al. 2017), emcee (Foreman-Mackey et al. 2013), pygtc (Bocquet & Carter 2016), matplotlib (Hunter 2007), IPAC forced Photometry Service.

REFERENCES

Ahn C. P., et al., 2012, ApJS, 203, 21
Alard C., Lupton R. H., 1998, ApJ, 503, 325
Amanullah R., et al., 2010, ApJ, 716, 712
Amanullah R., et al., 2014, ApJ, 788, L21
Amanullah R., et al., 2015, MNRAS, 453, 3300
Astier P., et al., 2006, A&A, 447, 31
Astropy Collaboration et al., 2013, A&A, 558, A33
Astropy Collaboration et al., 2018, AJ, 156, 123
Barbary K., et al., 2016, SNCosmo: Python library for supernova cosmology (ascl:1611.017)
Becker A., 2015, HOTPANTS: High Order Transform of PSF ANd Template Subtraction (ascl:1504.004)
Bellm E. C., et al., 2019a, PASP, 131, 018002
Bellm E. C., et al., 2019b, PASP, 131, 068003
Bertin E., 2010, SWarp: Resampling and Co-adding FITS Images Together (ascl:1010.068)
Betoule M., et al., 2014, A&A, 568, A22
Bocquet S., Carter F. W., 2016, The Journal of Open Source Software, 1, 46
Bourne N., et al., 2012, MNRAS, 421, 3027

Bradley L., et al., 2019, astropy/photutils: v0.6, doi:10.5281/zenodo.2533376
Brout D., Scolnic D., 2021, ApJ, 909, 26
Brout D., et al., 2019, ApJ, 874, 150
Bulla M., Goobar A., Dhawan S., 2018, MNRAS, 479, 3663
Burns C. R., et al., 2011, AJ, 141, 19
Burns C. R., et al., 2014, ApJ, 789, 32
Burns C. R., et al., 2020, ApJ, 895, 118
Byler N., Dalcanton J. J., Conroy C., Johnson B. D., 2017, ApJ, 840, 44
Calzetti D., Armus L., Bohlin R. C., Kinney A. L., Koornneef J., Storchi-Bergmann T., 2000, ApJ, 533, 682
Cardelli J. A., Clayton G. C., Mathis J. S., 1989, ApJ, 345, 245
Chabrier G., 2003, PASP, 115, 763
Chambers K. C., et al., 2016, arXiv e-prints, p. arXiv:1612.05560
Childress M., et al., 2013, ApJ, 770, 108
Chotard N., et al., 2011, A&A, 529, L4
Dettman K. G., et al., 2021, arXiv e-prints, p. arXiv:2102.06524
Foley R. J., et al., 2014, MNRAS, 443, 2887
Foley R. J., et al., 2018, MNRAS, 475, 193
Foreman-Mackey D., Hogg D. W., Lang D., Goodman J., 2013, PASP, 125, 306
Fremling C., et al., 2020, ApJ, 895, 32
Gagliano A., Narayan G., Engel A., Carrasco Kind M., LSST Dark Energy Science Collaboration 2021, ApJ, 908, 170
Galbany L., et al., 2012, ApJ, 755, 125
Goobar A., 2008, ApJ, 686, L103
Goobar A., Leibundgut B., 2011, Annual Review of Nuclear and Particle Science, 61, 251
Goobar A., et al., 2014, ApJ, 784, L12
Graham M. J., et al., 2019, PASP, 131, 078001
Guy J., Astier P., Nobili S., Regnault N., Pain R., 2005, A&A, 443, 781
Guy J., et al., 2007, A&A, 466, 11
Guy J., et al., 2010, A&A, 523, A7
Hayden B., Rubin D., Strovink M., 2019, ApJ, 871, 219
Hinton S. R., et al., 2019, ApJ, 876, 15
Hoang T., 2017, ApJ, 836, 13
Hoang T., 2021, ApJ, 907, 37
Hunter J. D., 2007, Computing in Science and Engineering, 9, 90
Ivezić Ž., et al., 2019, ApJ, 873, 111
Johansson J., et al., 2017, MNRAS, 466, 3442
Jones D. O., et al., 2018a, ApJ, 857, 51
Jones D. O., et al., 2018b, ApJ, 867, 108
Jones D. O., et al., 2021, ApJ, 908, 143
Kasliwal M. M., et al., 2019, PASP, 131, 038003
Kelly P. L., Hicken M., Burke D. L., Mandel K. S., Kirshner R. P., 2010, ApJ, 715, 743
Kelsey L., et al., 2021, MNRAS, 501, 4861
Kessler R., Scolnic D., 2017, ApJ, 836, 56
Kessler R., et al., 2009, ApJS, 185, 32
Kessler R., et al., 2013, ApJ, 764, 48
Kessler R., et al., 2019, MNRAS, 485, 1171
LSST Science Collaboration et al., 2009, arXiv e-prints, p. arXiv:0912.0201
Lampeitl H., et al., 2010, ApJ, 722, 566
Lang D., 2014, AJ, 147, 108
Léget P. F., et al., 2020, A&A, 636, A46
Leja J., Johnson B. D., Conroy C., van Dokkum P. G., Byler N., 2017, ApJ, 837, 170
Licquia T. C., Newman J. A., 2015, ApJ, 806, 96
Liddle A. R., 2007, MNRAS, 377, L74
Maeda K., Nozawa T., Nagao T., Motohara K., 2015, MNRAS, 452, 3281
Mainzer A., et al., 2014, ApJ, 792, 30
Marriner J., et al., 2011, ApJ, 740, 72
Masci F. J., et al., 2019, PASP, 131, 018003
Medford M. S., et al., 2021, arXiv e-prints, p. arXiv:2102.10738
Meisner A. M., Lang D., Schlegel D. J., 2017, AJ, 153, 38
Mosher J., et al., 2014, ApJ, 793, 16
Nataf D. M., et al., 2016, MNRAS, 456, 2692
Nobili S., Goobar A., 2008, A&A, 487, 19
Nordin J., Brinnel V., Giomi M., Santen J. V., Gal-Yam A., Yaron O., Schulze S., 2019, Transient Name Server Discovery Report, 2019-1202, 1
Nugent P., Kim A., Perlmutter S., 2002, PASP, 114, 803
Perley D. A., et al., 2020, ApJ, 904, 35
Perley D. A., Taggart K., Dahiwale A., Fremling C., 2021, Transient Name Server Classification Report, 2021-341, 1
Perlmutter S., et al., 1999, ApJ, 517, 565
Phillips M. M., 1993, ApJ, 413, L105
Piascik A. S., Steele I. A., Bates S. D., Mottram C. J., Smith R. J., Barnsley R. M., Bolton B., 2014, in Ramsay S. K., McLean I. S., Takami H., eds, Society of Photo-Optical Instrumentation Engineers (SPIE) Conference Series Vol. 9147, Ground-based and Airborne Instrumentation for Astronomy V. p. 91478H, doi:10.1117/12.2055117
Popovic B., Brout D., Kessler R., Scolnic D., Lu L., 2021, arXiv e-prints, p. arXiv:2102.01776
Riess A. G., et al., 1998, AJ, 116, 1009
Rigault M., 2018, ztfquery, a python tool to access ZTF data, doi:10.5281/zenodo.1345222
Rigault M., et al., 2015, ApJ, 802, 20
Rigault M., et al., 2020, A&A, 644, A176
Saunders C., et al., 2018, ApJ, 869, 167
Schulze S., et al., 2020, arXiv e-prints, p. arXiv:2008.05988
Schwarz G., 1978, Annals of Statistics, 6, 461
Scolnic D., Kessler R., 2016, ApJ, 822, L35
Scolnic D. M., et al., 2018, ApJ, 859, 101
Scolnic D., et al., 2020, ApJ, 896, L13
Skrutskie M. F., et al., 2006, AJ, 131, 1163
Soraisam M., Matheson T., Lee C.-H., 2021, arXiv e-prints, p. arXiv:2103.09937
Steele I. A., et al., 2004, in Oschmann Jacobus M. J., ed., Society of Photo-Optical Instrumentation Engineers (SPIE) Conference Series Vol. 5489, Ground-based Telescopes. pp 679–692, doi:10.1117/12.551456
Sullivan M., et al., 2010, MNRAS, 406, 782
Suzuki N., et al., 2012, ApJ, 746, 85
Thorp S., Mandel K. S., Jones D. O., Ward S. M., Narayan G., 2021, arXiv e-prints, p. arXiv:2102.05678
Tripp R., 1998, A&A, 331, 815
Tripp R., Branch D., 1999, ApJ, 525, 209
Wang L., 2005, ApJ, 635, L33
Wright E. L., et al., 2010, AJ, 140, 1868
Wright A. H., et al., 2016, MNRAS, 460, 765
van der Walt S., Colbert S. C., Varoquaux G., 2011, Computing in Science and Engineering, 13, 22

APPENDIX A: COMPARISON TO SNOOPY FITS

For comparison with the SNe Ia SALT2 colour model, we also infer the dust properties of the host galaxy using the SNooPy SN Ia

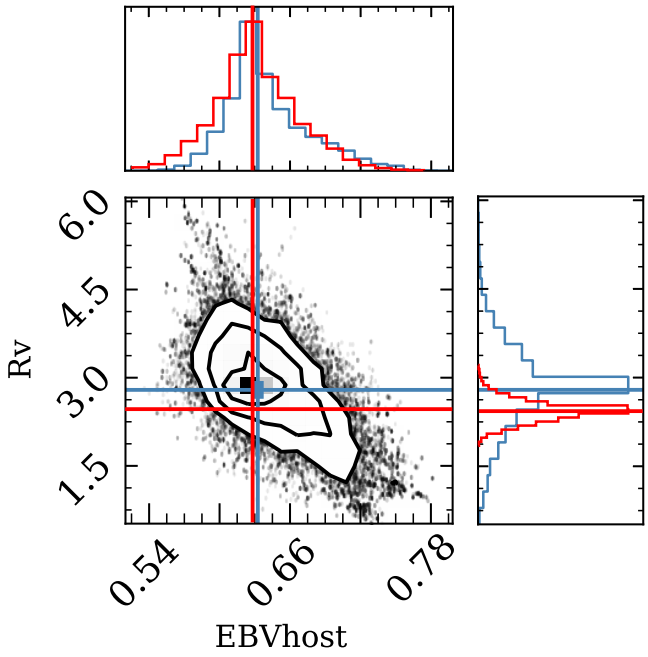

Figure A1. Contour plot showing the inferred R_V and $E(B-V)$ for AT2019lcj using the SNooPy SN model without any prior (black), with a prior on the unextinguished peak magnitude from SN2020aewj (red). The best fit $R_V = 2.8 \pm 0.7$ and $E(B-V) = 0.63 \pm 0.07$ mag without any prior and $R_V = 2.45 \pm 0.18$ and an $E(B-V) = 0.63 \pm 0.07$ with a prior on the peak apparent magnitude from SN 2020aewj.

model. SNooPy is a modular software with different SN Ia models, which can depend on various lightcurve shape parameters, to fit template lightcurves to SN Ia data. While models like the `max model` only fit for the peak magnitude in each filter, we use the `color model`, which also fits for the reddening parameters R_V and $E(B-V)$. The color model templates are a function of the colour-stretch, s_{BV}, which is the time since maximum when the $B-V$ colour curve reaches its maximum value, normalised to 30 d. The s_{BV} parameter is shown to be a better ordering parameter than the conventional Δm_{15} lightcurve shape, especially for fast-declining SNe Ia (Burns et al. 2014). Fitting the SNooPy colour model to the g, r, i data for AT2019lcj yields an $R_V = 2.8 \pm 0.71$ and $E(B-V) = 0.63 \pm 0.07$ mag (see Figure A1. Additionally, similar to the procedure with the SALT2 colour-luminosity and use a prior on the apparent reddening corrected magnitude of AT2019lcj from the model fit to SN2020aewj. This yields an $R_V = 2.45 \pm 0.18$ and an $E(B-V) = 0.63 \pm 0.07$ mag. The R_V values from the SNooPy fit are consistent well within 1 σ with the $\beta - 1$ from the SALT2 fits.

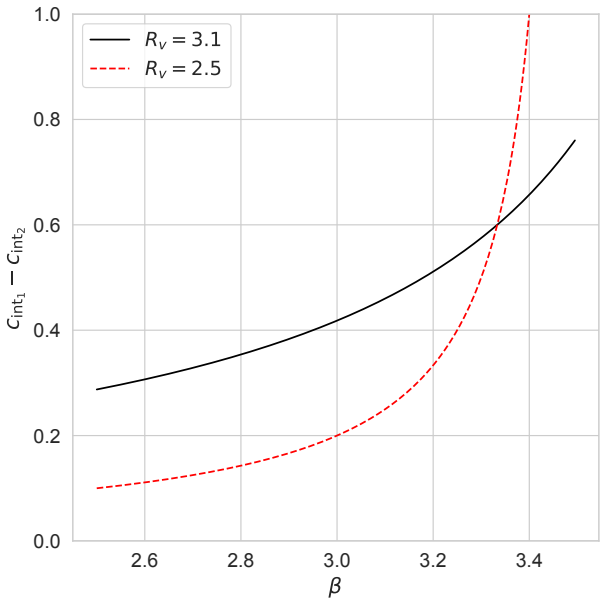

Figure B1. The differences in c_{int} in the model described in Brout & Scolnic (2021) for the pair of siblings described as a function of β (note that this is different from the Tripp model β constrained in Sec. 4 for two choices of R_V.

APPENDIX B: THE DUST MODEL IN BROUT & SCOLNIC (2021)

Brout & Scolnic (2021) propose a change to the prevalent `SALT2` methodology positing that the `SALT2` colour parameter c obtained from light curve fits is the sum of two terms

$$c_{SALT} = c_{int} + E_{dust} \tag{B1}$$

where E_{dust} is the redenning due to the host galaxy dust and is constrained to be positive, while c_{int} is a colour intrinsic to the supernova. Accordingly, they modify the Tripp Ansatz

$$\mu = m - M + \alpha \cdot x_1 - \beta \cdot c \tag{B2}$$

to

$$\mu = m - M + \alpha \cdot x_1 - \beta \cdot c_{int} - R_B \cdot E_{dust} \tag{B3}$$

demonstrating that a correlation between R_B and stellar mass of the host galaxy can account for the observed host correlations. A side-effect is that the population distribution of c_{int} is a fairly narrow Gaussian with a mean of 0.084 and standard deviation of 0.042. Thus, the well known red tail in supernova populations (see for example, Scolnic & Kessler (2016)) is interpreted as being due to higher values of E_{dust} in this model.

In the context of the current work, this model is different from the standard `SALT2` model and Tripp Ansatz . It has more free parameters, and clearly has a different physical interpretation from the stanardard `SALT2` and Tripp relations. In fact, here β which has a universal value is completely independent of R_B, which varies from host galaxy to host galaxy. Brout & Scolnic (2021) demonstrate that a correlation between stellar masses of galaxies and R_B coud drive the observed correlations between the standardized brightnesses of SN Ia and their host galaxies. We note

that the stellar mass of the host galaxy of the siblings is comparable to that of the Milky Way, and thus one might expect this galaxy to have a similar R_V as the Milky Way based on this model.

While we postpone a proper analysis of this model to future work, we can set the SALT2 parameters to the maximum likelihood of the SALT2 parameters as recorded in Tab. 1. Approximating the individual fits in Tab. 1, as the difference of SALT2 c parameters is 0.57, the difference in $x1 \sim 0$, and the difference in $m_B^\star$ as ~ 2, we fix these parameeters. Using Eqn. B1 and Eqn. 4 to eliminate the terms involving E_{dust}, this imposes a relationship between the remaining variables $\alpha, \beta, R_B, c_{int}$. Utilizing the Pantheon Priors on α, this gives us the difference in c_{int}, $\Delta c_{int} = c_{int}^1 - c_{int}^2$ for different values of R_B and β. In Fig. B1, we show the values of Δc_{int} for different choices β where we have fixed R_V to 3.1 or 2.5. Since we know the population distribution of c_{int} is a normal distribution of known mean and variance, we can see that the pdf of the Δc_{int} is a normal distribtion with mean approximately 1.6 and a standard deviation of 0.06.

APPENDIX C: PHOTOMETRY TABLES USED

Note these tables are also made available in electronic format.

This paper has been typeset from a TEX/LATEX file prepared by the author.

Table C1. Light curve points for AT 2019lcj used in the analysis. The zero points are in the AB system.

jd (days)	band	flux (counts)	flux_err (counts)	zp	seeing(″)	$m_{\rm lim}$ (mag)
2458655.79	p48g	18.72	37.23	25.93	2.9745	19.91
2458662.94	p48g	56.02	22.66	26.06	1.9512	20.79
2458663.97	p48g	65.35	35.57	25.58	2.1306	19.75
2458663.97	p48g	-58.13	36.12	25.54	2.174	19.64
2458672.81	p48g	143.99	18.31	26.02	2.4073	20.73
2458672.83	p48g	93.51	18.66	26.04	1.9574	20.96
2458673.80	p48g	181.56	23.37	26.09	2.2867	20.62
2458673.83	p48g	167.44	19.76	26.08	1.9766	20.94
2458674.83	p48g	216.91	28.24	26.11	1.779	20.64
2458674.85	p48g	266.67	22.44	26.08	2.0647	20.74
2458675.81	p48g	183.23	36.75	26.07	1.9471	20.28
2458675.85	p48g	243.35	31.69	26.06	1.8856	20.45
2458678.78	p48g	369.44	52.74	26.06	2.6459	19.58
2458679.79	p48g	354.50	58.68	26.09	2.1964	19.67
2458680.70	p48g	497.51	65.23	26.08	2.1413	19.58
2458681.70	p48g	353.79	66.10	26.07	2.3575	19.46
2458682.70	p48g	416.38	51.36	26.09	2.0582	19.86
2458683.78	p48g	404.32	49.62	26.09	1.9435	19.96
2458684.77	p48g	412.83	41.90	25.99	2.5365	19.86
2458685.87	p48g	430.13	43.94	26.02	2.2696	19.90
2458693.77	p48g	353.75	22.05	26.05	2.2308	20.69
2458696.76	p48g	275.83	22.50	26.08	1.998	20.75
2458696.81	p48g	278.77	22.62	26.06	1.9962	20.75
2458697.83	p48g	250.44	23.89	26.04	1.865	20.72
2458699.81	p48g	165.57	24.34	26.01	2.0476	20.63
2458700.76	p48g	236.76	23.21	26.07	2.0132	20.70
2458700.81	p48g	252.79	23.53	26.05	1.8405	20.75
2458701.81	p48g	112.43	23.90	25.96	1.9193	20.62
2458702.81	p48g	145.08	24.18	25.97	1.8191	20.65
2458703.69	p48g	106.19	34.28	25.93	2.6593	19.99
2458703.81	p48g	201.14	24.65	25.99	1.9368	20.61
2458704.81	p48g	136.22	34.00	26.01	2.3005	20.13
2458704.88	p48g	122.88	26.77	25.89	2.7116	20.19
2458704.90	p48g	134.62	27.42	25.87	2.7151	20.12
2458705.73	p48g	127.43	41.91	26.03	1.7947	20.16
2458705.91	p48g	163.97	27.59	25.88	2.4236	20.22
2458706.68	p48g	123.65	45.22	26.11	1.951	20.07
2458706.73	p48g	46.97	46.01	26.03	1.928	20.04
2458707.91	p48g	125.95	48.56	25.97	2.0606	19.81
2458708.66	p48g	97.68	55.14	26.07	1.6609	19.93
2458708.73	p48g	189.82	55.55	26.05	2.2432	19.69
2458708.89	p48g	-9.06	62.65	25.97	2.0441	19.52
2458709.73	p48g	151.77	61.24	26.10	1.9602	19.70
2458710.66	p48g	206.42	63.87	26.10	1.6057	19.83
2458710.71	p48g	97.73	68.72	26.10	2.0118	19.56
2458710.73	p48g	92.19	69.68	26.05	1.9891	19.54
2458711.71	p48g	72.08	62.48	26.08	1.7558	19.78
2458711.76	p48g	77.31	65.87	26.07	1.8454	19.67
2458714.71	p48g	67.30	37.72	26.04	1.8598	20.27
2458715.80	p48g	15.07	42.89	26.02	1.8539	20.10
2458716.82	p48g	47.07	40.81	26.00	1.9475	20.10
2458717.80	p48g	106.93	34.90	25.98	2.1284	20.18
2458718.82	p48g	80.48	31.08	25.91	2.5508	20.10
2458719.80	p48g	85.00	26.32	25.90	2.511	20.25
2458720.82	p48g	45.66	27.68	25.90	1.8968	20.43
2458722.80	p48g	67.01	26.90	25.96	1.7849	20.55
2458725.68	p48g	59.00	24.40	25.94	2.5194	20.40
2458725.70	p48g	117.88	24.53	26.02	2.1454	20.57
2458725.80	p48g	66.25	26.46	26.01	1.895	20.58
2458726.80	p48g	8.70	27.05	25.94	2.2034	20.38
2458727.77	p48g	40.43	26.43	25.97	1.8142	20.57
2458727.82	p48g	12.92	28.40	25.93	1.9406	20.41
2458728.68	p48g	57.67	25.33	25.96	1.6413	20.65
2458730.80	p48g	16.70	28.23	25.85	2.0934	20.28

Table C1 – *continued* Light curve points for AT 2019lcj used in the analysis

2458732.65	p48g	48.68	34.33	25.98	1.8434	20.29
2458732.68	p48g	19.28	34.25	25.98	1.6656	20.36
2458732.69	p48g	8.11	33.99	25.97	1.8042	20.32
2458732.79	p48g	29.79	26.97	25.95	1.7882	20.54
2458733.66	p48g	11.55	36.81	26.03	1.9404	20.25
2458733.79	p48g	96.79	33.92	25.89	2.5993	19.92
2458733.81	p48g	61.58	31.29	25.91	2.3659	20.11
2458733.83	p48g	45.68	29.15	25.84	2.6269	20.05
2458734.69	p48g	91.92	39.74	25.96	2.7377	19.85
2458734.72	p48g	13.64	40.51	25.92	2.9513	19.74
2458734.80	p48g	33.17	40.78	25.95	2.3262	19.85
2458735.79	p48g	59.31	47.94	25.93	2.1473	19.74
2458736.80	p48g	3.06	55.10	25.85	2.8398	19.33
2458659.68	p48i	-98.84	37.22	25.52	1.3288	19.98
2458663.68	p48i	-39.71	28.13	25.45	1.8868	19.90
2458672.94	p48i	131.23	30.23	25.48	1.8611	19.90
2458679.76	p48i	438.90	36.02	25.56	1.5662	19.96
2458685.80	p48i	293.17	35.28	25.52	1.461	19.98
2458690.83	p48i	391.43	31.57	25.48	1.4088	20.12
2458696.68	p48i	230.51	31.10	25.52	1.4778	20.15
2458701.91	p48i	180.12	35.62	25.41	1.4528	19.91
2458710.75	p48i	166.77	44.15	25.54	1.5235	19.73
2458715.81	p48i	237.98	35.97	25.51	1.6284	19.90
2458719.66	p48i	216.90	33.67	25.46	1.6936	19.86
2458732.83	p48i	144.40	33.99	25.42	1.6258	19.83
2458654.86	p48r	76.85	44.48	26.02	2.2151	19.92
2458657.87	p48r	-43.84	33.28	26.04	1.9803	20.39
2458661.83	p48r	-98.84	25.44	26.05	1.9287	20.69
2458661.83	p48r	9.59	24.91	26.05	2.0323	20.70
2458662.75	p48r	13.14	28.98	26.08	1.7381	20.59
2458663.83	p48r	-80.74	28.56	26.05	2.013	20.54
2458663.84	p48r	-6.23	28.78	26.06	1.966	20.56
2458663.84	p48r	30.49	29.50	26.09	1.6037	20.67
2458665.85	p48r	24.15	28.52	26.11	1.5575	20.70
2458672.72	p48r	207.37	29.31	26.05	1.9369	20.51
2458673.72	p48r	358.72	31.29	26.13	1.4066	20.64
2458677.77	p48r	550.80	45.17	26.09	1.5020	20.26
2458678.72	p48r	681.85	47.77	26.12	1.4399	20.24
2458679.74	p48r	773.15	50.47	26.12	1.5577	20.15
2458680.76	p48r	734.08	54.11	26.08	2.1612	19.77
2458681.76	p48r	753.90	55.16	26.06	2.2524	19.73
2458682.76	p48r	683.84	49.04	26.12	1.489	20.18
2458683.75	p48r	782.34	44.65	26.10	1.5661	20.27
2458684.74	p48r	697.07	37.29	26.02	2.2422	20.15
2458685.84	p48r	830.17	40.62	26.09	1.5865	20.32
2458688.89	p48r	864.20	38.46	26.03	1.523	20.34
2458690.85	p48r	677.57	32.01	26.02	1.3362	20.56
2458691.68	p48r	723.03	29.70	26.05	1.53	20.62
2458692.83	p48r	594.66	32.16	26.04	1.6437	20.50
2458693.72	p48r	574.09	31.92	26.03	1.5733	20.55
2458694.70	p48r	579.28	30.94	26.10	1.395	20.68
2458695.78	p48r	355.74	38.66	25.21	1.9794	19.30
2458696.78	p48r	609.70	28.70	26.09	1.5222	20.70
2458696.86	p48r	468.21	29.53	26.06	1.6503	20.60
2458697.80	p48r	529.99	29.90	26.06	1.7317	20.59
2458699.78	p48r	456.27	31.49	26.05	1.5015	20.56

Table C1 – *continued* Light curve points for AT 2019lcj used in the analysis

2458701.78	p48r	345.30	35.18	25.78	1.7682	20.08
2458702.78	p48r	313.64	33.10	25.96	1.3461	20.48
2458703.68	p48r	344.44	36.48	26.00	1.9797	20.24
2458703.78	p48r	464.35	34.31	26.03	1.7509	20.39
2458704.78	p48r	322.64	37.13	26.03	2.2181	20.11
2458705.68	p48r	416.77	41.75	26.06	1.7215	20.24
2458705.70	p48r	595.86	42.53	26.07	1.4837	20.30
2458706.70	p48r	510.31	43.66	26.10	1.4447	20.29
2458706.84	p48r	415.71	46.48	26.05	1.5837	20.16
2458707.70	p48r	371.49	46.63	26.09	1.4241	20.26
2458709.70	p48r	426.38	53.09	26.09	1.7109	20.03
2458710.69	p48r	354.46	57.26	26.10	1.4671	20.01
2458711.69	p48r	334.41	52.62	26.11	1.5541	20.07
2458714.69	p48r	441.02	33.92	26.07	1.5714	20.55
2458715.77	p48r	219.52	40.72	26.08	1.486	20.34
2458716.79	p48r	275.66	40.50	26.06	1.654	20.28
2458717.77	p48r	335.43	35.88	26.05	1.6434	20.41
2458718.79	p48r	185.96	33.32	25.99	2.1706	20.25
2458719.77	p48r	115.37	33.86	25.91	2.6513	20.00
2458720.79	p48r	262.36	34.92	25.99	1.5167	20.42
2458722.77	p48r	340.10	33.25	26.03	1.4654	20.50
2458723.80	p48r	95.53	32.70	26.01	1.6926	20.50
2458725.77	p48r	245.73	32.49	26.06	1.3984	20.56
2458726.77	p48r	235.97	34.85	26.04	1.5069	20.49
2458727.80	p48r	186.60	35.37	26.02	1.4836	20.42
2458730.64	p48r	107.54	38.77	25.96	1.6622	20.23
2458730.77	p48r	152.84	37.58	25.93	1.8356	20.15
2458732.77	p48r	107.84	36.56	26.04	1.3995	20.44
2458733.74	p48r	199.48	39.83	26.07	1.7258	20.28
2458733.77	p48r	11.14	41.14	26.04	1.7149	20.23
2458734.77	p48r	116.41	43.88	26.02	1.8755	20.06
2458734.82	p48r	130.66	44.73	25.94	2.3806	19.78
2458736.78	p48r	108.34	52.57	25.99	1.9647	19.84
2458737.79	p48r	94.51	57.59	25.98	2.1669	19.64

Table C2. Light curve points for SN 2020aewj used in the analysis. The zero points are in the AB system.

jd (days)	band	flux (counts)	flux_err (counts)	zp	seeing(″)	$m_{\rm lim}$ (mag)
2458877.02	p48g	742.07	27.51	26.08	2.6403	20.24
2458880.98	p48g	1473.84	28.76	25.99	2.7017	20.21
2458882.02	p48g	2005.69	27.94	26.12	2.2046	20.49
2458891.97	p48g	2594.26	60.44	26.08	2.5028	19.51
2458893.99	p48g	2401.47	46.10	26.09	2.1244	19.95
2458899.05	p48g	2023.54	26.14	26.18	1.9566	20.74
2458900.04	p48g	1777.22	27.06	26.10	2.427	20.38
2458901.04	p48g	773.74	33.82	25.33	2.0688	19.53
2458904.03	p48g	1337.40	24.73	26.15	2.0789	20.73
2458909.05	p48g	852.24	44.56	26.16	2.3004	19.96
2458912.05	p48g	600.80	33.44	26.03	2.8533	20.06
2458914.02	p48g	456.64	26.50	25.93	2.0779	20.46
2458914.94	p48g	400.14	58.13	25.97	2.0866	19.56
2458915.97	p48g	443.95	66.20	26.03	2.2789	19.43
2458942.00	p48g	187.59	20.76	26.00	2.8643	20.53
2458874.03	p48r	320.95	34.97	26.14	1.8541	20.46
2458876.05	p48r	457.65	30.19	26.04	2.5855	20.24
2458877.06	p48r	735.35	34.38	26.18	1.7229	20.54
2458878.02	p48r	887.10	32.10	26.10	2.205	20.34
2458879.07	p48r	947.57	45.33	25.98	2.8889	19.71
2458881.04	p48r	1502.91	34.15	26.11	2.2954	20.29
2458882.05	p48r	1827.11	34.74	26.15	1.8957	20.46
2458886.05	p48r	2295.86	36.98	26.14	2.0698	20.35
2458887.06	p48r	2408.75	49.58	26.19	1.6498	20.22
2458888.05	p48r	2480.49	63.14	26.18	1.7269	19.90
2458894.05	p48r	2516.26	45.71	26.17	1.5729	20.34
2458895.04	p48r	2546.97	42.90	26.18	1.6562	20.37
2458895.99	p48r	2402.58	39.21	26.16	1.8695	20.35
2458899.03	p48r	2148.01	32.88	26.17	1.5319	20.67
2458899.98	p48r	1840.99	36.65	26.10	2.4675	20.10
2458904.01	p48r	1585.96	32.71	26.16	1.8345	20.59
2458908.99	p48r	1382.19	34.75	26.14	1.9151	20.46
2458912.99	p48r	1361.77	38.80	26.09	1.7249	20.39
2458914.00	p48r	975.57	39.22	25.84	1.5394	20.18
2458937.02	p48r	598.16	36.08	26.13	1.784	20.48
2458941.01	p48r	288.69	38.65	25.73	1.8366	19.96